JURNAL KIMIA VALENSI
p-ISSN: 2460-6065; e-ISSN: 2548-3013
Journal homepage: https://journal.uinjkt.ac.id/index.php/valensi
Research Article

Hybrid $CaO/ZnFe_2O_4$ Modified with Al_2O_3 as a Green Catalyst for Biodiesel Production from Waste Cooking Oil

Jenia Villa Hapsari, Helmiyati*, Yuni K. Krisnandi

Department of Chemistry, Faculty of Mathematics and Natural Sciences, Universitas Indonesia, Pondok Cina, Beji, Depok City, 16424, Indonesia

Email: helmiyati@sci.ui.ac.id

Article Info
Received: Dec 14, 2023
Revised: Jan 04, 2024
Accepted: April 22, 2024
Online: May 31, 2024

Citation:
Hapsari, J. V., Helmiyati, & Krisnandi, Y. K. (2024). Hybrid $CaO/ZnFe_2O_4$ Modified with Al_2O_3 as a Green Catalyst for Biodiesel Production from Waste Cooking Oil. *Jurnal Kimia Valensi*, 10(1), 1–10.

Doi:
10.15408/jkv.v10i1.36594

Abstract
In this work, biodiesel was produced from waste cooking oil (WCO) via a green catalyst of $CaO-ZnFe_2O_4$ modified Al_2O_3. The catalyst was characterized using Fourier-transform infrared spectroscopy (FTIR), X-ray powder diffraction (XRD), scanning electron microscopy (SEM), energy dispersive x-ray (EDX), SEM-mapping, Brunauer-Emmett-Teller (BET), transmission electron microscopy (TEM) analyses. The catalyst performance was studied in the transesterification reaction of WCO conversion to biodiesel. The catalytic activity increased with the combination of nanoparticles effect and support catalysts obtained biodiesel yield of nano-Al_2O_3, nano-CaO, $ZnFe_2O_4$, $CaO-ZnFe_2O_4$, and $CaO-ZnFe_2O_4/Al_2O_3$ is 36.86%, 67.16%, 74.83%, 86.54%, and 93.41%, respectively. The best biodiesel yield was 93.41% with a mass ratio of Al_2O_3 to $CaO-ZnFe_2O_4$ (2:1). The physicochemical properties (acid number, density, kinematic viscosity, flash point, and cetane number) of biodiesel under the optimal conditions agreed with the ASTM standard. These results show that the developed nanocomposite has great potential to reduce biodiesel production costs because derived from WCO. In conclusion, $CaO-ZnFe_2O_4$ modified Al_2O_3 as a catalyst has a high potential for biodiesel production on a large scale.

Keywords: Biodiesel; catalyst; nanocomposite; transesterification; waste cooking oil

1. INTRODUCTION

In the last few years, energy issues have grown due to global demand worldwide. The depletion of fossil energy sources and the growth of environmental pollution were the main contributing factors to renewable energy development[1,2]. Biodiesel is a renewable alternative energy substitute for fossil fuels, it reduces greenhouse gasses and is non-toxic, and biodegradable[3]. Biodiesel is obtained through the triglyceride transesterification reaction from fatty acids such as edible feedstocks, non-edible feedstocks, and waste feedstocks such as waste cooking oils (WCO) with low-chain alcohols in the presence of a catalyst[4,5]. The use of WCO is a very efficient effort to deal with waste problems by processing them into renewable energy sources [6].

An important factor associated with biodiesel production is the use of catalysts in synthesis. This fuel large-scale production occurs using mostly homogeneous catalysts, such as NaOH, KOH, etc. However, homogeneous catalysts are difficult to separate, corrosive, and environmentally harmful [7]. Heterogeneous catalysts are an alternative to these problems because of their favorable characteristics such as high selectivity, regeneration ease of separation from the reaction mixture, and the potential to be reused[8–10]. Among the heterogeneous catalysts in biodiesel synthesis, calcium oxide (CaO) exhibits high activity in transesterification[11]. Besides, it is environmentally friendly and can be synthesized from less valuable residues, namely eggshells, animal bones, snail shells, oyster shells, etc[12–14].

However, the disadvantages of CaO are mainly from natural sources that have low stability causing the degradation of the structure of CaO and can dissolve in the biodiesel phase. To improve the catalytic activity and stability of calcium oxide, it is necessary to modify CaO with other metal oxides, including combining magnetic catalysts, so that can be separated by an external magnetic field[15]. Metal-ferrite nanoparticles or MFe_2O_4

(M=Co, Ni, Mg, Cu, etc) have many benefits including high surface area, great reusability, tunable size, high stability, and magnetic features[16,17]. Besides that, to increase the surface area the catalyst can be combined with a catalyst support, including zeolite, silica, and alumina (Al_2O_3)[18]. Alumina is one of the support catalysts suitable for efficient biodiesel production due to its high specific surface area, porous structure, and high stability[19].

Several studies with heterogeneous bases CaO for transesterification in biodiesel production have been investigated, like Hybrid CaO/Al_2O_3 aerogelsF; Novel SrO/$MgFe_2O_4$ magnetic nanocatalysts at low temperatures[20]; A novel robust CaO/$ZnFe_2O_4$ hollow magnetic microspheres with yeast templates[21]; Metal loading on CaO/Al_2O_3 pellet catalyst[22]; Aluminum industrial waste as a precursor of efficient CaO/Al_2O_3 nano-catalyst[18]; Mg decorated $CoFe_2O_4$ nanocatalyst[23]; Hybrid CuO/Al_2O_3 nanoparticles[24].

Based on previous research, this paper combines ideas from previous research with new modifications in the preparation of the heterogeneous catalyst-based calcium oxide of chicken eggshell combined by hollow structure $ZnFe_2O_4$ using yeast cells as a biotemplate and alumina as a supported catalyst. Therefore, the purpose of this study is to synthesize a catalyst using Al_2O_3 as a support combined with a CaO and $ZnFe_2O_4$ composite which will be used as a catalyst in the transesterification process of waste cooking oil (WCO) into biodiesel or fatty acid methyl ester (FAME). Furthermore, the novel catalyst was characterized by X-ray diffraction (XRD), Fourier-transform infrared spectroscopy (FT-IR), Brunauer-Emmett-Teller (BET), scanning electron microscopy (SEM), energy diffraction X-ray (EDX), Elemental distribution mappings by SEM, and transmission electron microscopy (TEM).

2. RESEARCH METHODS

Materials and Instruments

The materials used in this research were chicken eggshell waste as nano-CaO source, $Fe(NO_3)_3 \cdot 9H_2O$, $Zn(NO_3)_2 \cdot 6H_2O$ as $ZnFe_2O_4$ precursors, ($Al(NO_3)_3 \cdot 9H_2O$) as Al_2O_3 precursor, CH_3OH were procured from Merck, and WCO as the feedstock for biodiesel, yeast was obtained from the local market.

The instruments used were Fourier transform infrared spectrophotometer (FTIR) Alpha II-Bruker, X-ray diffraction (XRD) Panalytical Empyrean X-ray diffraction, scanning electron microscope (SEM) FEI Quanta 650 scanning electron microscope, Brunauer-Emmett-Teller (BET) quantachrome quadrasorb-evo surface area and pore size analyzer, and transmission electron microscopy (TEM) FEI Tecnai G2 SuperTwin TEM/STEM.

2.1 Synthesis of nano-CaO

Nano-CaO was prepared from chicken eggshell waste using the previously reported method[25], the collected chicken eggshells were extensively washed with distilled water and dried for 2 h in an oven at 110 °C, then ground through a ball milling process. The samples were calcined for 3 h at 900 °C with a heating rate of 10 °C/min.

2.2 Synthesis of $ZnFe_2O_4$ Hollow Structure

The synthesis of $ZnFe_2O_4$ was prepared as a previously reported method[21]. In the first stage, 2 g of yeast cells used as bio-template was dissolved in 50 ml of distilled water and stirred for 20 min to ensure complete dispersion of yeast cells. In the next stage, $FeNO_3 \cdot 9H_2O$ and $Zn(NO_3)_2 \cdot 6H_2O$ were added with constant stirring at 60 °C for 1 h. Then, 25% liquid ammonia solution was added drop by drop until the pH of the solution reached between 9 and 10. The precipitate was separated, washed with distilled water, and dried in an oven at 60 °C for 12 h.

2.3 Synthesis of nano-Al_2O_3

Nano-Al_2O_3 was prepared as a previously reported method[26]. A 0.5 M $Al(NO_3)_3 \cdot 9H_2O$ was dissolved in 40 mL of distilled water and 120 mL of 1.5 M NH_4OH was added drop by drop by stirring using a magnetic stirrer for 20 min at 60 °C. The white precipitate was filtered and washed using distilled water and ethanol, dried at 100 °C for 2 h, and calcined at 550 °C for 5 h.

2.4 Synthesis of CaO-$ZnFe_2O_4$ Composite

Synthesis of CaO-$ZnFe_2O_4$ using the coprecipitation method as previously reported[21]. The $ZnFe_2O_4$ hollow nanostructures were dispersed in distilled water by ultrasonic waves. The resulting dispersion supplemented with nano-CaO was slowly stirred and adjusted with 2 M NaOH to reach a pH of 12. The mixture was stirred continuously at 600 rpm, 60 °C for 3 h. The product was separated, washed with distilled water, and dried at 60 °C.

2.5 Synthesis of CaO-$ZnFe_2O_4$/Al_2O_3 Nanocomposite

Nanocomposite of CaO-$ZnFe_2O_4$/Al_2O_3 was prepared using a slight modification of a previously reported method[27]. In the first stage, CaO-$ZnFe_2O_4$ composite was added to a solution of 10 mL of 0.25 M NaOH and slowly stirred for 1 h (mixture A). In the second stage, nano-Al2O3 in 50 mL of distilled water and slowly stirred for 1 h (mixture B). Then mixture A was added slowly to mixture B and stirred at 27 °C for 6 h. The resulting mixture was filtered and rinsed using water and ethanol, dried at 100 °C for 2 h, and calcined at 550 °C for 5 h.

2.6 Preparation of Waste Cooking Oil (WCO)

WCO preparation refers to the previous method[28]. The WCO was filtered to remove impurities with gauze, then the washing process was done with warm water with a weight ratio water to WCO of 10:1 stirred for 30 min, and left overnight so that the water and oil phases could be separated. The resulting WCO added silica gel and stirred for 3 h followed by vacuum filtration using Whatman filter paper to remove the silica gel. The WCO is stored in a tightly closed bottle.

2.7 Catalytic activity

The catalytic activity was tested as described in previous studies[29]. The experiments were done in a 100 ml glass reactor equipped with a condenser and a mechanical stirrer, this system is submerged in a water bath under controlled temperature. In a typical test, 2 wt% catalyst was added to WCO and methanol (methanol to WCO molar ratio 9:1). The mixture was refluxed by stirring at different temperatures and times. After the reaction, the catalyst was separated by an external magnet. The products are transferred to a funnel to separate the two phases of biodiesel and glycerol. Biodiesel yield was calculated in Eq (1)[30].

$$\text{Biodiesel yield (\%)} = \frac{Weight\ of\ biodiesel}{Weight\ of\ WCO} \times 100 \qquad (1)$$

3. RESULTS AND DISCUSSION

3.1 Synthesis of CaO-$ZnFe_2O_4/Al_2O_3$ Nanocomposite

The use of Al_2O_3 as a catalyst support is used to increase the number of active groups, surface area, and catalytic efficiency of nanocomposites with CaO and $ZnFe_2O_4$. The role of yeast as a template in the synthesis of $ZnFe_2O_4$ is to create a hollow structure in the $ZnFe_2O_4$ that will be formed. This will cause an increase in surface area compared to $ZnFe_2O_4$ which does not have a hollow structure.

3.2 Characterization

3.2.1 FTIR Analysis

The molecular vibration of catalysts was analyzed by Fourier Transform Infrared spectroscopy (FTIR) in the range of 400–4000 cm^{-1}. **Figure 1** shows the FTIR spectra of nano-CaO, $ZnFe_2O_4$, nano-Al_2O_3, CaO-$ZnFe_2O_4$ composite, and CaO-$ZnFe_2O_4/Al_2O_3$ nanocomposite. The FTIR spectra of nano-CaO have an intense peak at 874 cm^{-1} related to the stretching of the Ca-O bond and a wide peak at 512 cm^{-1}, which is a typical characteristic of Ca-O nanoparticles[31]. The sharp peak at 3640 cm^{-1} may be assigned to the OH stretching for $Ca(OH)_2$ the due to absorption of water by CaO[22,32] (**Figure 1a**). The FTIR spectra of $ZnFe_2O_4$ with a yeast template have a peak around 420 cm^{-1} related to the stretching of Zn-O bond and around 501 cm^{-1} attributed to the Fe- O bond. The width peak around 3410 cm^{-1} could be attributed to the overlap of hydroxyl and amine

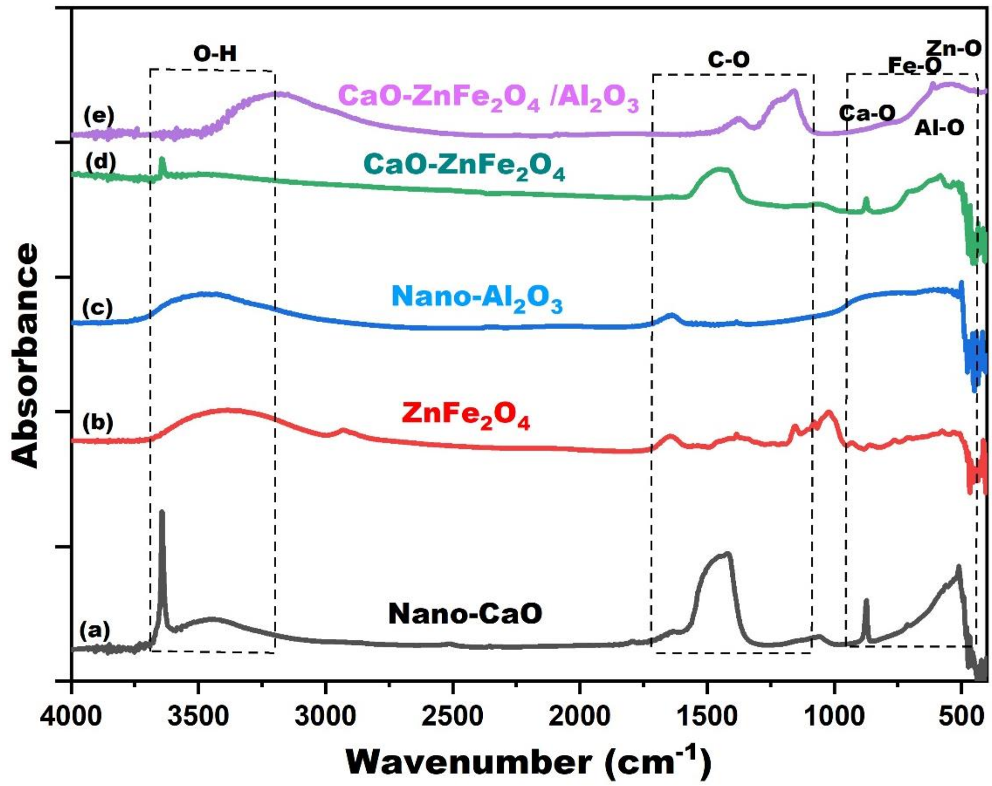

Figure 1. FTIR spectra of (a) CaO, (b) $ZnFe_2O_4$, (c) Al_2O_3, (d) CaO-$ZnFe_2O_4$, and (e) CaO-$ZnFe_2O_4/Al_2O_3$

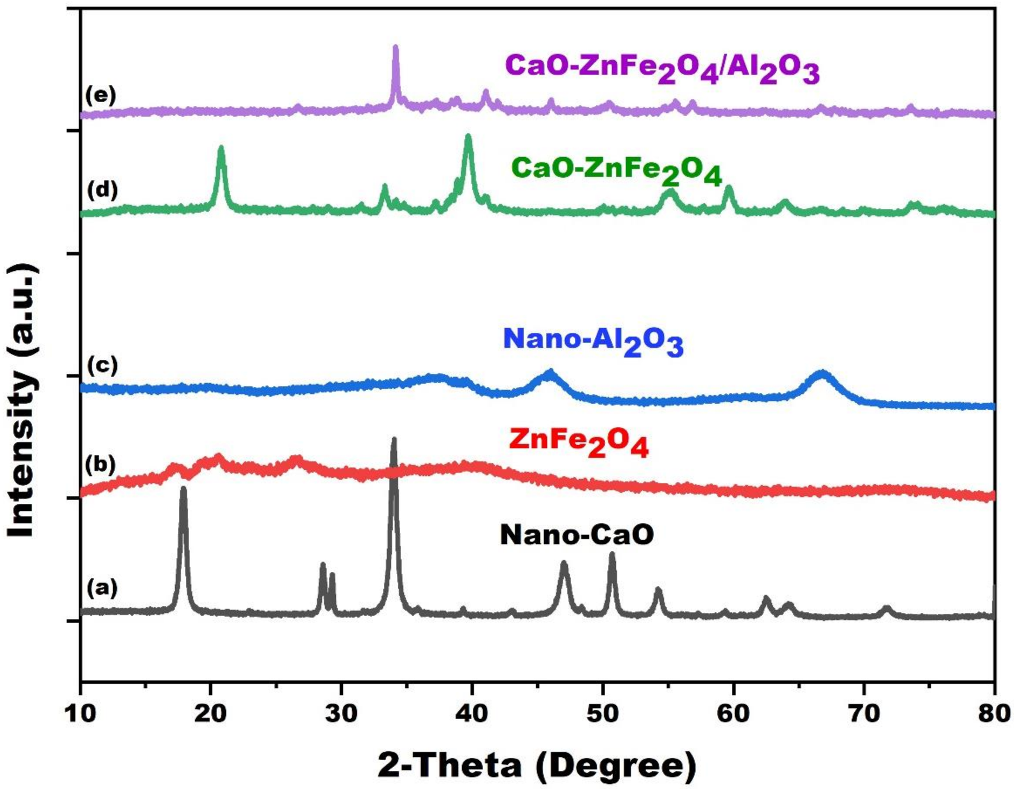

Figure 2. XRD patterns of (a) $ZnFe_2O_4$, (b) Al_2O_3, (c) CaO, (d) CaO-$ZnFe_2O_4$, (e) CaO-$ZnFe_2O_4$/Al_2O_3

functional groups. The peak at 2926 cm^{-1} shows C–H asymmetric stretching and around 1491 cm^{-1} appointed to the amide group confirmed the presence of the protein in yeast cells[21] (**Figure 1b).** The FTIR spectra of nano-Al_2O_3 show a peak around 529 cm^{-1} related to the stretching of an Al-O bending vibration, which is a typical peak for nano-alumina, and around 1384 cm^{-1} there is the bending vibration of the hydroxyl group[33] (**Figure 1c**). **Figure** 1d shows the spectra of the CaO-$ZnFe_2O_4$ composite which has combined absorption peaks from CaO and $ZnFe_2O_4$, namely vibrations from Ca-O, Zn-O, and Fe-O. Furthermore, **Figure 1e** shows that the CaO-$ZnFe_2O_4$/Al_2O_3 nanocomposite spectra and indicate combined peaks from nano-CaO, $ZnFe_2O_4$, and nano-Al_2O_3. However, the nanocomposite does not show a sharp peak, possibly due to the groups being embedded in the pores of the alumina support.

3.2.2 XRD Analysis

XRD patterns and crystalline structures of nano-CaO, $ZnFe_2O_4$, nano-Al_2O_3, CaO-$ZnFe_2O_4$, and compared with CaO-$ZnFe_2O_4$/Al_2O_3 nanocomposites as shown in **Figure 2**. The characteristic peak of nano-CaO at 2θ: 17.98°, 28.56°, 34.13°, 47.17°, 50.82°, 54.22°, 64.14°, respectively. The results of the diffractogram analysis of CaO nanoparticles are in agreement with JCPDS No. 48-1467[22] (**Figure 2a)**. **Figure 2b** shows the typical peaks of $ZnFe_2O_4$ at 2θ: 17.22°, 20.53°, 26.73°, 39.35°, 41.98°, 73.64°, respectively. These results are similar to previous research [21]. **Figure 2c** shows the typical peak of nano-Al_2O_3 at 2θ: 37.15°, 45.86°, 66.61°, respectively. These results are similar to previous research[19]. **Figure** 1d shows the diffraction pattern of the CaO-$ZnFe_2O_4$ composite which has combined peaks from CaO and $ZnFe_2O_4$. Furthermore, **Figure 1e** shows the diffraction pattern of CaO-$ZnFe_2O_4$/Al_2O_3 nanocomposite and indicates combined peaks from nano-CaO, $ZnFe_2O_4$, and nano-Al_2O_3. However, the nanocomposite does not show a sharp peak, possibly due to the groups being embedded in the pores of the alumina support, this is similar to the FTIR spectra. The average crystal size of CaO-$ZnFe_2O_4$/Al_2O_3 calculated using the Debye Scherrer equation[34] was obtained as 23.52 nm.

3.2.3 SEM Analysis

The surface morphology was investigated using SEM shown in **Figure 3**. The nano-CaO have irregular non-uniform and porous (**Figure 3A**), in accordance with previous research[32,35]. $ZnFe_2O_4$ hollow structure has granular irregular non-uniform, these results are similar to previous studies [21] (**Figure 3B**). The nano-Al_2O_3 has irregular non-uniform and shows pores (**Figure 3C**). Meanwhile, the CaO-$ZnFe_2O_4$ composite (**Figure 3D**)

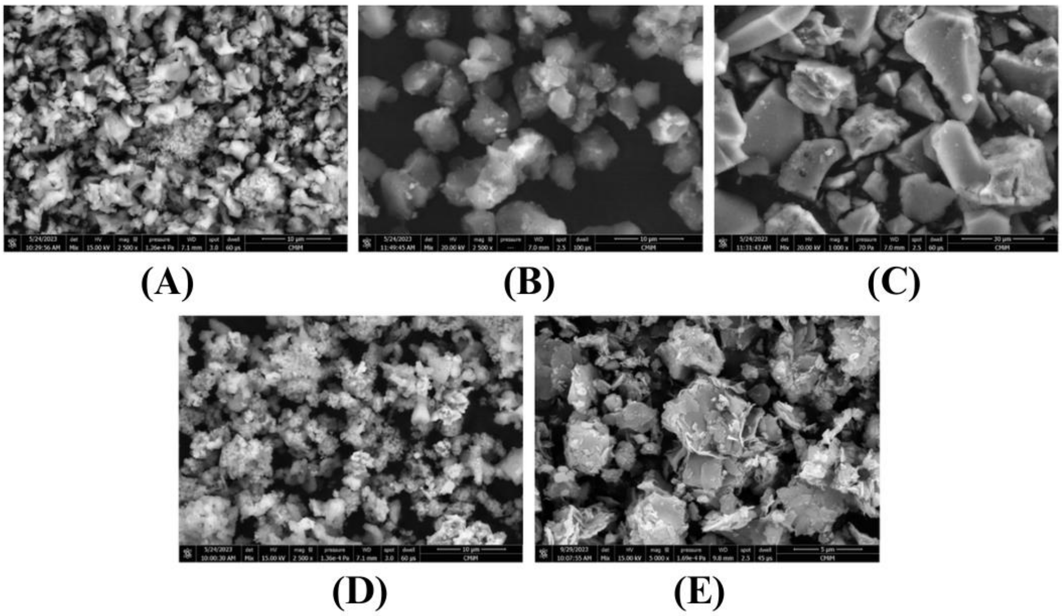

Figure 3. SEM images of (A) CaO, (B) $ZnFe_2O_4$, (C) Al_2O_3, (D) CaO-$ZnFe_2O_4$, (E) CaO-$ZnFe_2O_4$/Al_2O_3

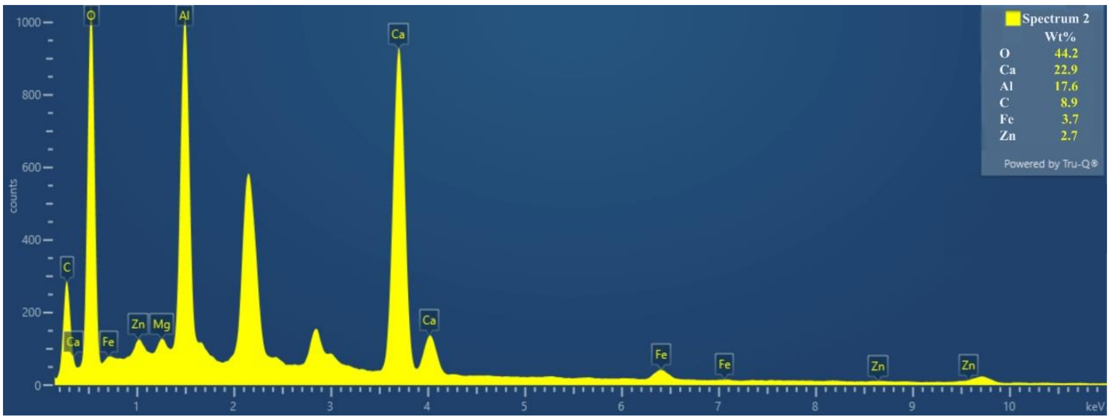

Figure 4. SEM EDX spectrum of CaO-$ZnFe_2O_4$/Al_2O_3

shows that there are particles that have a granular structure arranged irregularly, indicating the presence of CaO and $ZnFe_2O_4$ for CaO- $ZnFe_2O_4$ composite, and shown in **Figure 3E**, the composite of CaO-$ZnFe_2O_4$ composite have combined with Al_2O_3 forming nanocomposite. Based on **Figure 4**, it can be identified that the elements that make up the CaO-$ZnFe_2O_4$/Al_2O_3 nanocomposite are O, Ca, Al, C, Fe, and Zn with a mass percentage of 4.2%, 22.9%, 17.6%, 8.9%, 3.7%, and 2.7%, respectively. The distribution of CaO-$ZnFe_2O_4$ on the Al_2O_3 surface was observed by elemental mapping (**Figure 5**). **Figure 5A–G** shows that the constituent elements are evenly distributed on the surface of CaO-$ZnFe_2O_4$/Al_2O_3, and CaO-$ZnFe_2O_4$ is also evenly distributed on the surface of Al_2O_3, which confirms the successful synthesis of the CaO-$ZnFe_2O_4$/Al_2O_3 nanocomposite.

3.2.4 BET Analysis

The N_2 sorption isotherms of CaO-$ZnFe_2$O4 and CaO-$ZnFe_2O_4$/Al_2O_3 (**Figure 6**) show typical type IV isotherms indicating the presence of mesopores for pores with diameters in the range of 2–50 nm[20]. **Figure 6** displays the results of the BET surface area and pore volume for the CaO-$ZnFe_2O_4$ composite and CaO-$ZnFe_2O_4$/Al_2O_3 nanocomposite showing that CaO-$ZnFe_2O_4$/Al_2O_3 has a higher BET surface area (134.426 m^2g^{-1}) and pore volume (0.204 cm^3g^{-1}) compared to CaO-$ZnFe_2O_4$ (15.314 m^2g^{-1}) and a pore volume of 0.022 cm^3g^{-1}). These surface area results indicate that the addition of alumina as a support for the CaO-$ZnFe_2O_4$ composite succeeded in increasing the surface area after it was formed into a CaO-$ZnFe_2O_4$/Al_2O_3 nanocomposite.

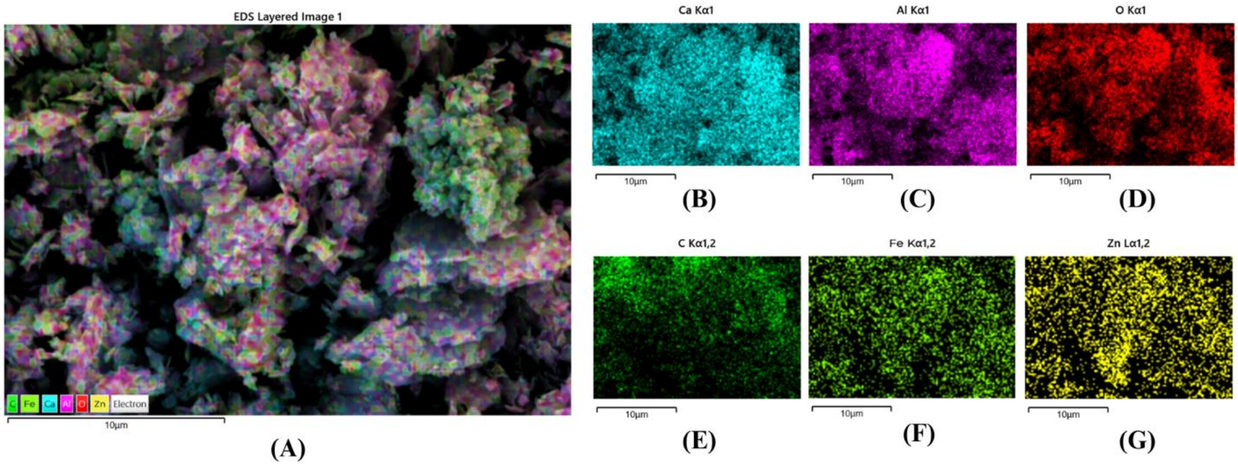

Figure 5. Elemental distribution mappings [(A) overall elemental of $CaO-ZnFe_2O_4/Al_2O_3$, (B) Ca, (C) Al, (D) O, (E) C, (F) Fe, and (G) Zn]

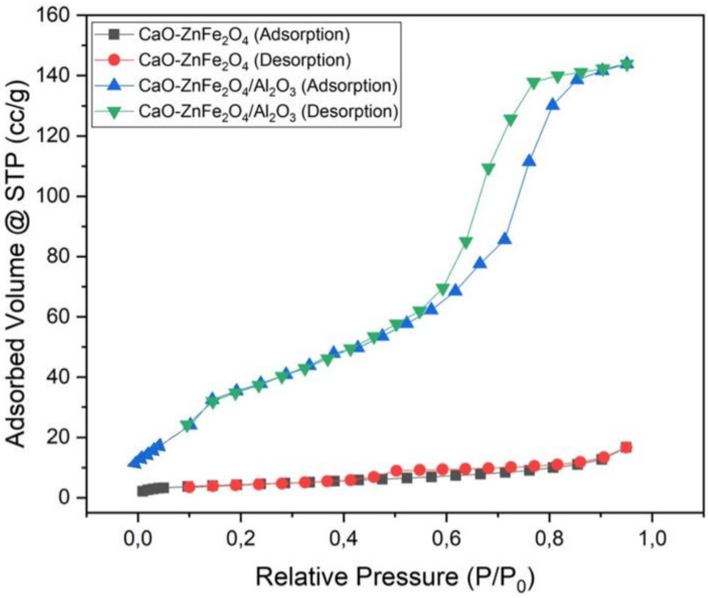

Figure 6. N_2 sorption isotherms curves of $CaO-ZnFe_2O_4$ and $CaO-ZnFe_2O_4/Al_2O_3$

3.2.5 TEM Analysis

The results of TEM characterization are shown in **Figure 7**. **Figure 7A-B** shows the surface morphology of $CaO-ZnFe_2O_4/Al_2O_3$ with scales of 500 nm and 100 nm, respectively. The $CaO-ZnFe_2O_4/Al_2O_3$ nanocomposite shows that its constituent particle components have bonded one each other. The $CaO-ZnFe_2O_4$ composite with a non-uniform shape (the dark colors) attached to the Al_2O_3 surface (the bright colors) was observed clearly in Figure 7B. **Figure 7C** presents a high-resolution TEM image of $CaO-ZnFe_2O_4/Al_2O_3$ on a scale of 10 nm.

3.3 Catalytic Activity of $CaO-ZnFe_2O_4/Al_2O_3$

The catalytic activity for the conversion of waste cooking oil into biodiesel was investigated for 2 h at a temperature of 65 °C using a quantity of waste cooking oil of 5 mL, with catalyst amount of 2%, and the volume ratio of waste cooking oil: methanol of 1:9.

3.3.1 Effect of Al_2O_3: $CaO-ZnFe_2O_4$ Mass Ratio on Biodiesel Yield

The structure of alumina as catalyst support has a high surface area desired site active $CaO-ZnFe_2O_4$ to evenly spread on the pore surface, resulting in enhanced catalytic activity. Therefore, we investigated the influence of the mass ratio of Al_2O_3 to $CaO-ZnFe_2O_4$ in $CaO-ZnFe_2O_4/Al_2O_3$ nanocomposites (**Figure 8**). The biodiesel yield obtained using a catalyst of Al_2O_3/ $CaO-ZnFe_2O_4$ mass ratio 1:1; 1:2; and 1:3 is 80.43%, 93.41%, and 90.14%, respectively. This shows that at the 2:1 mass ratio, the entire surface of the Al_2O_3 pores is filled by the active site and is evenly distributed, resulting in efficient biodiesel production. Therefore, the Al_2O_3/ $CaO-ZnFe_2O_4$ with a mass ratio of 2:1 provides optimal conditions for this transesterification reaction.

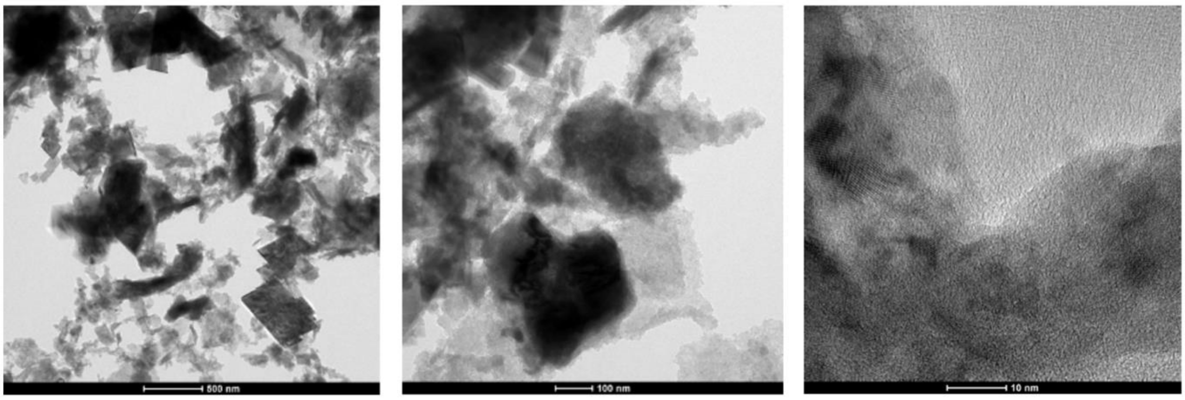

(A) (B) (C)

Figure 7. TEM image of $CaO\text{-}ZnFe_2O_4/Al_2O_3$ (a) 500 nm and (b) 100 nm, HR TEM image of $CaO\text{-}ZnFe_2O_4/Al_2O_3$ (c) 10 nm

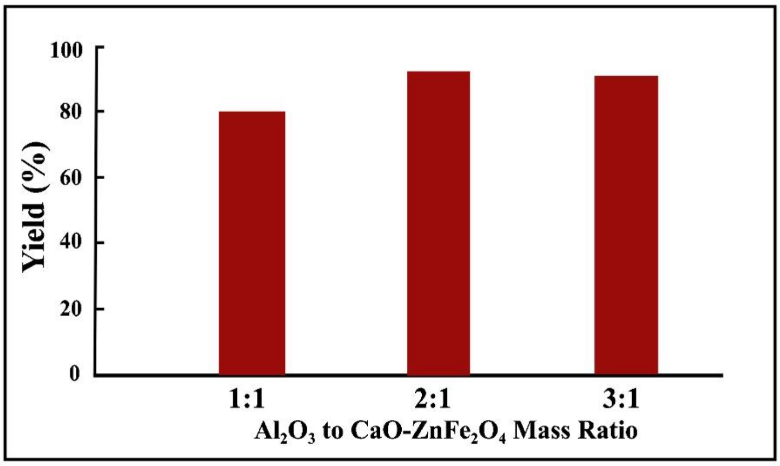

Figure 8. Effect of Al_2O_3 to $CaO\text{-}ZnFe_2O_4$ mass ratio on percent yield

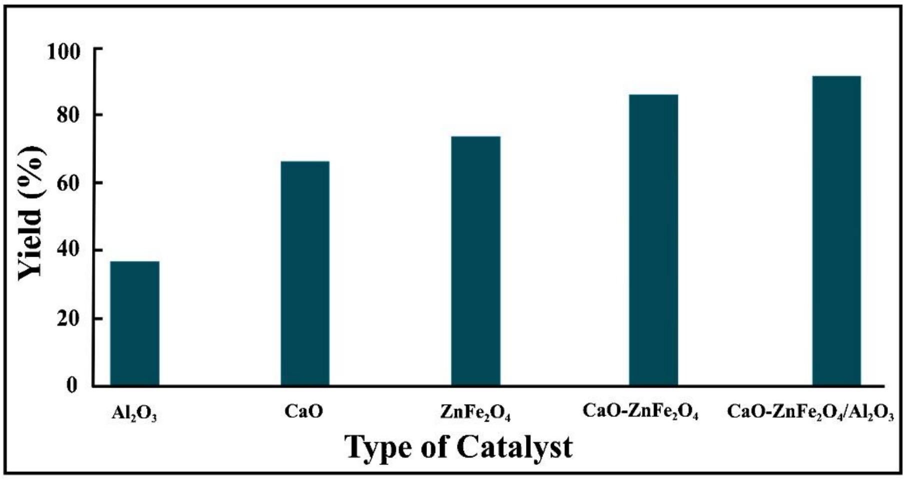

Figure 9. Effect of type catalyst on percent yield

3.3.2 Effect of Catalyst Type on Biodiesel Yield

Subsequently, we investigated the effect of catalyst type on the biodiesel yield as shown in **Figure 9**. The usage of the nano-Al_2O_3 support catalyst achieved a biodiesel yield of 36.86%, nano-CaO catalyst of 67.16%, $ZnFe_2O_4$ of 74.83%, $CaO\text{-}ZnFe_2O_4$ of 86.54% and CaO- $ZnFe_2O_4/Al_2O_3$ nanocomposite of 93.41%. The biodiesel yield uses the $CaO\text{-}ZnFe_2O_4$ catalyst increases compared to the nano-CaO and $ZnFe_2O_4$. This is due to $CaO\text{-}ZnFe_2O_4$ having both acidic and basic properties, which are the base site (CaO) and acid site ($ZnFe_2O_4$). The acid-base properties of the $CaO\text{-}ZnFe_2O_4$ hollow structure could accelerate the transesterification and esterification reaction[21]. Hence, CaO-$ZnFe_2O_4/Al_2O_3$ catalyst has the highest biodiesel yield. These indicate that the supported catalyst of the Al_2O_3 in nanocomposite can increase biodiesel yield due to the Al_2O_3 having a high surface area compared to CaO-

Table 1. Physical properties of biodiesel obtained in this work.

Physical Properties	Biodiesel product	ASTM 6751
Acid number (mg KOH/g)	0.530	<0.80
Density (g/mL) at 25 °C	0.873	0.85–0.90
Kinematic viscosity ($mm^{2/}s$) at 40 °C	3.92	1.00–6.00
Flash point (°C)	125	100-170
Cetane number	49.00	>47

$ZnFe_2O_4$ (**Figure 6**) and acid-base properties of the $CaO/ZnFe_2O_4$ to the synergistic effect between CaO-$ZnFe_2O_4$ and Al_2O_3.

3.4 Physicochemical Properties of Biodiesel

The results of biodiesel with the best and optimal have been done to test some physicochemical properties to be a suitable substitute for fossil diesel[36,37]. Some properties of biodiesel tested in this study are acid number, density, kinematic viscosity, flash point, and cetane number. **Table 1** displays that these properties are close to the required international standards as specified by the American Society for Testing Materials (ASTM) 6751 reference standard.

4. CONCLUSIONS

In this study, hybrid $CaO/ZnFe_2O_4$ modified with Al_2O_3 as a green novel catalyst for biodiesel production from WCO with high catalytic activity. The catalyst properties were investigated by FTIR, XRD, SEM, EDX, SEM-mapping, BET, and TEM analyses. The catalytic activity increased with the combination of nanoparticles effect and support catalysts obtained biodiesel yield of nano-Al_2O_3, nano-CaO, $ZnFe_2O_4$, CaO-$ZnFe_2O_4$, and CaO-$ZnFe_2O_4/Al_2O_3$ is 36.86%, 67.16%, 74.83%, 86.54%, and 93.41%, respectively. The best biodiesel yield was 93.41% with a mass ratio of Al_2O_3 to CaO-$ZnFe_2O_4$ (2:1). The physicochemical properties (acid number, density, kinematic viscosity, flash point, and cetane number) of the produced biodiesel were within the ASTM limits, demonstrating a promising replacement with diesel.

Acknowledgments

This work was supported through the Postgraduate PUTI Grant, University of Indonesia, number: NKB-226/UN2.RST/HKP.05.00/2023.

REFERENCES

1. Dey S, Reang NM, Das PK, Deb M. A comprehensive study on prospects of economy, environment, and efficiency of palm oil biodiesel as a renewable fuel. *J Clean Prod*. 2021;286. doi:10.1016/j.jclepro.2020.124981
2. Basahel SN, Ali TT, Mokhtar M, Narasimharao K. Influence of crystal structure of nanosized ZrO2 on photocatalytic degradation of methyl orange. *Nanoscale Res Lett*. 2015;10(1). doi:10.1186/s11671-015-0780-z
3. Helmiyati H, Budiman Y, Abbas GH, Dini FW, Khalil M. Highly efficient synthesis of biodiesel catalyzed by a cellulose@hematite-zirconia nanocomposite. *Heliyon*. 2021;7(3). doi:10.1016/j.heliyon.2021.e06622
4. Sandouqa A, Al-hamamre Z. Economical evaluation of jojoba cultivation for biodiesel production in Jordan. *Renew Energy*. 2021;177:1116-1132. doi:10.1016/j.renene.2021.06.025
5. Helmiyati, Anggraini Y. Nanocomposites comprising cellulose and nanomagnetite as heterogeneous catalysts for the synthesis of biodiesel from oleic acid. *Int J Technol*. 2019;10(4):798-807. doi:10.14716/ijtech.v10i4.2597
6. Chen Q, Wang A, Quan W, Gong W. Efficient synthesis of biodiesel from Hyoscyamus niger L . seed oil by base catalysis. *Fuel Process Technol*. 2023;241(December 2022):107630. doi:10.1016/j.fuproc.2022.107630
7. Ferreira GF, Fregolente LV. Sustainable catalysts for biodiesel production : The potential of CaO supported on sugarcane bagasse biochar. *Renew Sustain Energy Rev*. 2024;189(May 2023):114042. doi:doi.org/10.1016/j.rser.2023.114042
8. Al-saadi A, Mathan B, He Y. Chemical Engineering Research and Design Biodiesel production via simultaneous transesterification and esterification reactions over SrO – ZnO / Al 2 O 3 as a bifunctional catalyst using high acidic waste cooking oil. *Chem Eng Res Des*. 2020;162(2018):238-248. doi:10.1016/j.cherd.2020.08.018
9. Munyentwali A, Li H, Yang Q. Applied Catalysis A , General Review of advances in bifunctional solid acid / base catalysts for sustainable biodiesel production. 2022;633(November 2021). doi:10.1016/j.apcata.2022.118525
10. Dini FW, Helmiyati H, Krisnandi YK. Cellulose and TiO2–ZrO2 nanocomposite as a catalyst for

glucose conversion to 5-EMF. *Bull Chem React Eng Catal*. 2021;16(2):320-330. doi:10.9767/bcrec.16.2.10320.320-330

11. Maafa IM, Sayed AA, El-magied MOA, Cui X, Dhmees AS. Eco-friendly self-terminated process for preparation of CaO catalyst based on chitosan production wastes for biodiesel production. *J Mater Res Technol*. 2024;30(January):1217-1227. doi:doi.org/10.1016/j.jmrt.2024.03.091
12. Erchamo YS, Mamo TT, Workneh GA. Improved biodiesel production from waste cooking oil with mixed methanol – ethanol using enhanced eggshell - derived CaO nano - catalyst. *Sci Rep*. Published online 2021:1-12. doi:10.1038/s41598-021-86062-z
13. Marinkovi M, Waisi H, Blagojevi S, Zarubica A. The effect of process parameters and catalyst support preparation methods on the catalytic efficiency in transesterification of sunflower oil over heterogeneous KI / Al 2 O 3 -based catalysts for biodiesel production. 2022;315(November 2021). doi:10.1016/j.fuel.2022.123246
14. Sudana IW, Helmiyati, Yunarti RT. Alginate-CMC/Fe 3 O 4 -CaO nanocomposite as a catalyst for synthesis of biodiesel from waste cooking oil. *IOP Conf Ser Earth Environ Sci*. 2021;846(1):012008. doi:10.1088/1755-1315/846/1/012008
15. Karami S, Zeynizadeh B. Reduction of 4-nitrophenol by a disused adsorbent: EDA-functionalized magnetic cellulose nanocomposite after the removal of Cu 2+. *Carbohydr Polym*. 2019;211(August 2018):298-307. doi:10.1016/j.carbpol.2019.01.113
16. Tamjidi S, Kamyab B, Esmaeili H. Ultrasound-assisted biodiesel generation from waste edible oil using CoFe 2 O 4 @ GO as a superior and reclaimable nanocatalyst : Optimization of two-step transesterification by RSM. *Fuel*. 2022;327(June):125170. doi:doi.org/10.1016/j.fuel.2022.125170
17. Tabesh F, Mallakpour S, Mustansar C. Recent advances in magnetic semiconductor ZnFe 2 O 4 nanoceramics : History , properties , synthesis , characterization , and applications. *J Solid State Chem*. 2023;322(February). doi:doi.org/10.1016/j.jssc.2023.123940
18. Abu-ghazala AH, Abdelhady HH, Mazhar AA, El- MS. Enhanced low-temperature production of biodiesel from waste cooking oil : aluminum industrial waste as a precursor of efficient CaO / Al 2 O 3. *Fuel*. 2023;351(January):128897. doi:doi.org/10.1016/j.fuel.2023.128897
19. Kesserwan F, Ahmad MN, Khalil M, El-rassy H. Hybrid CaO / Al 2 O 3 aerogel as heterogeneous catalyst for biodiesel production. *Chem Eng J*. 2020;385(December 2019):123834. doi:doi.org/10.1016/j.cej.2019.123834
20. Mawlid OA, Abdelhady HH, El-Deab MS. Boosted biodiesel production from waste cooking oil using novel SrO/MgFe2O4 magnetic nanocatalyst at low temperature: Optimization process. *Energy Convers Manag*. 2022;273(October). doi:10.1016/j.enconman.2022.116435
21. Torkzaban S, Feyzi M. A novel robust CaO / ZnFe 2 O 4 hollow magnetic microspheres heterogenous catalyst for synthesis biodiesel from waste frying sunflower oil. *Renew Energy*. 2022;200(October):996-1007. doi:10.1016/j.renene.2022.09.077
22. Chanthon N, Munbupphachart N, Ngaosuwan K, Kiatkittipong W, Wongsawaeng D, Mens W. Metal loading on CaO / Al 2 O 3 pellet catalyst as a booster for transesterification in biodiesel production. *Renew Energy*. 2023;218(May):119336. doi:doi.org/10.1016/j.renene.2023.119336
23. Yang X, Liu W, Zhao R, Raise A. Industrial Crops & Products Enhanced conversion of non-edible Jatropha oil to biodiesel utilizing highly reusable Mg decorated CoFe 2 O 4 nanocatalyst : Optimization by RSM. *Ind Crop Prod*. 2023;204(PB):117319. doi:10.1016/j.indcrop.2023.117319
24. Abdulnabi A, Al-iessa H, Abdollahi A, Soleimanimehr H. Investigating the atomic and thermal performance of soy biodiesel methyl ester in the presence of hybrid CuO / Al 2 O 3 nanoparticles by molecular dynamics simulation. *Eng Anal Bound Elem*. 2023;151(February):8-18. doi:doi.org/10.1016/j.enganabound.2023.02.038
25. El-sherif AA, Hamad AM, Shams-eldin E, et al. Power of recycling waste cooking oil into biodiesel via green CaO-based eggshells / Ag heterogeneous nanocatalyst. *Renew Energy*. 2023;202(December 2022):1412-1423. doi:doi.org/10.1016/j.renene.2022.12.041
26. Ali S. Synthesis of g-alumina (Al2O3) nanoparticles and their potential for use as an adsorbent in the removal of methylene blue dye from industrial wastewater. *Nanoscale Adv*. 2019;(1):213-218. doi:10.1039/c8na00014j
27. Zhang Y, Niu S, Han K, Li Y, Lu C. Synthesis of the SrO e CaO e Al 2 O 3 trimetallic oxide catalyst for transesteri fi cation to produce biodiesel. *Renew Energy*. 2021;168:981e990. doi:doi.org/10.1016/j.renene.2020.12.132
28. Liu Y, Yang X, Zhu Z. Economic evaluation and production process simulation of biodiesel production from waste cooking oil. *Curr Res Green Sustain Chem*. Published online 2021:100091. doi:10.1016/j.crgsc.2021.100091

29. Collins E, Wang Z, Yu Y, Callistus U, Duan P, Kapusta K. Industrial Crops & Products Yield optimization and fuel properties evaluation of the biodiesel derived from avocado pear waste. *Ind Crop Prod*. 2023;191(PA):115884. doi:10.1016/j.indcrop.2022.115884
30. Harsha Hebbar HR, Math MC, Yatish K V. Optimization and kinetic study of CaO nano-particles catalyzed biodiesel production from Bombax ceiba oil. *Energy*. 2018;143:25-34. doi:10.1016/j.energy.2017.10.118
31. Ajala EO, Ajala MA, Odetoye TE, Aderibigbe FA. Thermal modification of chicken eggshell as heterogeneous catalyst for palm kernel biodiesel production in an optimization process. *Biomass Convers Biorefinery*. 2020;11:2599-2615. doi:doi.org/10.1007/s13399-020-00636-x
32. Helmiyati H, Masriah I. Preparation of cellulose/CaO-Fe2O3 nanocomposites as catalyst for fatty acid methyl ester production. In: *AIP Conference Proceedings*. Vol 2168. American Institute of Physics Inc.; 2019. doi:10.1063/1.5132489
33. Farahmandjou M, Khodadadi A, Yaghoubi M. Low Concentration Iron-Doped Alumina (Fe / Al 2 O 3) Nanoparticles Using Co-Precipitation Method. *J Supercond Nov Magn*. 2020;33:3425–3432. doi:doi.org/10.1007/s10948-020-05569-0
34. Hossain S, Ahmed S. Easy and green synthesis of TiO 2 (Anatase and Rutile): Estimation of crystallite size using Scherrer equation , Williamson-Hall plot , Monshi-Scherrer Model , size-strain plot , Halder- Wagner Model. *Results Mater*. 2023;20(November):100492. doi:/doi.org/10.1016/j.rinma.2023.100492
35. Khatibi M, Khorasheh F, Larimi A. Biodiesel production via transesteri fi cation of canola oil in the presence of Na e K doped CaO derived from calcined eggshell. *Renew Energy*. 2021;163:1626-1636. doi:10.1016/j.renene.2020.10.039
36. Helmi F, Helmi M, Hemmati A. Phosphomolybdic acid/chitosan as acid solid catalyst using for biodiesel production from pomegranate seed oil via microwave heating system: RSM optimization and kinetic study. *Renew Energy*. 2022;189:881-898. doi:10.1016/j.renene.2022.02.123
37. Bukkarapu KR, Krishnasamy A. A critical review on available models to predict engine fuel properties of biodiesel. *Renew Sustain Energy Rev*. 2022;155(November 2021):111925. doi:doi.org/10.1016/j.rser.2021.111925